Rare Metal Materials and Engineering
Volume 52, Issue 3, March 2023
Available online at www.rmme.ac.cn

Science Press

Cite this article as: Mao Binyang, Liu Ying, Ye Jinwen, et al. Effect of Scanning Speed on Surface Roughness and Mechanical Properties of 316L Stainless Steel Prepared by Selective Laser Melting[J]. Rare Metal Materials and Engineering, 2023, 52(03): 860-866.

ARTICLE

Effect of Scanning Speed on Surface Roughness and Mechanical Properties of 316L Stainless Steel Prepared by Selective Laser Melting

Mao Binyang, Liu Ying, Ye Jinwen, Chen Zhengjie

College of Materials Science and Engineering, Sichuan University, Chengdu 610065, China

Abstract: The 316L stainless steel part was prepared by the selective laser melting method at different scanning speeds. The effects of scanning speed on phase constitution, molten pool morphology, surface roughness, density, and mechanical properties of the part were investigated by phase analyses, metallographic microscopy, tensile test, Vickers hardness test, and surface roughness test. Results show that all specimens are successfully prepared at different scanning speeds (800–1200 mm/s). In addition, with increasing the scanning speed, the ratio of depth to width of molten pool without remelting is decreased, and the surface roughness is increased from 5.78 μm to 22.79 μm. The cracks appear at scanning speed of 800 mm/s, while the molten line shrinkage occurs when the scanning speed exceeds 1100 mm/s. When the scanning speed is 800 mm/s, specimens have relatively high porosity due to the overhigh laser input energy. When the scanning speed is 900 mm/s, the specimens have the optimal Vickers hardness (2401 MPa) and high relative density (99.2%).

Key words: selective laser melting; 316L; surface roughness; scanning speed

Additive manufacturing plays an increasingly important role in modern industry due to its unique advantages in fabrication of metallic materials[1]. Among the additive manufacturing techniques, selective laser melting (SLM) is considered as a promising method to produce parts with complex internal structures[2] in a short period. Therefore, SLM has received great attention and is widely used in aerospace, automotive, and biomedical[3] fields in industrial production[4–5]. Austenitic 316L stainless steel has been widely used in industry due to its excellent performance of ductility, strength, and corrosion resistance[6], which is one of the most commonly used alloys in additive manufacturing.

During SLM process, the powder is melted by laser beam and a single molten pool is formed. As the laser beam moves, the molten pools connect together, forming a molten line. Then, the molten lines combine, forming a thin metal layer. With the accumulation of metal layers, a three-dimensional printed part is formed. Every step has a significant influence on the final performance of the printed part. Yadroitsev et al[7] reported that more than 10 processing parameters can affect the manufacture of printed parts. Among them, laser power, scanning speed, hatch distance, and layer thickness have been widely researched. Le et al[8] found that the high-deep molten pool is more likely to form pores than the medium-deep molten pool. Bertoli et al[9] studied the influence of scanning speed on the morphology of the molten line and found that with increasing the scanning speed, the wettability of molten pool is decreased and the contact angle of molten pool is increased. Therefore, the morphology of molten lines changes from a relatively flat and wide profile to a tall and narrow one under fast scanning speed. Guo et al[10] suggested that the high laser power input can lead to cracks on the surface of molten lines, and the cracks are perpendicular to the scanning direction of laser beam. Sun et al[11] found that the increase in laser power results in the high depth-to-width ratio of molten pool, which changes the crystallographic texture of the printed parts.

Changes in processing parameters can also affect the

Received date: August 31, 2022
Foundation item: National Key Research and Development Plan of China (2017YFB0305900); Sichuan Science and Technology Program (2020ZDZX0008)
Corresponding author: Liu Ying, Ph. D., Professor, College of Materials Science and Engineering, Sichuan University, Chengdu 610065, P. R. China, Tel: 0086-28-85405332, E-mail: liuying5536@scu.edu.cn

Copyright © 2023, Northwest Institute for Nonferrous Metal Research. Published by Science Press. All rights reserved.

performance of printed parts. Song et al[12] reported that increasing the scanning speed is harmful to the yield strength of printed parts. Additionally, Tucho et al[13] confirmed that the hardness of print parts is decreased with increasing the scanning speed. Cherry et al[14] concluded that the insufficient energy input may increase the porosity of SLM materials.

SLM material is composed of metal layers. The thickness of the powder layer has a remarkable impact on the performance of printed parts. Even under the same SLM process parameters, the increasing thickness of powder layer can weaken the hardness but increase the surface roughness of the printed parts[15].

Although the influence of SLM process parameters on the morphology of single molten line has been extensively researched, the surface roughness of the printed parts is rarely discussed. In this research, the effects of scanning speed on hardness and surface roughness of 316L stainless steel after SLM were studied. In addition, a printing model was designed to observe the cross section of the molten pool without remelting.

1 Experiment

The morphology of 316L stainless steel powder observed by scanning electron microscope (SEM) is shown in Fig. 1. The diameter D_{10}, D_{50}, and D_{90} of 316L powder is 12, 32, and 65 μm, respectively. The particle size of 316L powder is in uniform distribution, as shown in Fig. 2. The chemical composition of 316L powder is listed in Table 1.

A 3D metal printer (EOS M290, German) was used to prepare SLMed specimens in this experiment, as shown in Fig.3. Fig.3a shows the profile of equipment system. Recoater was used to feed powder, and the substrate was connected to the printed part to provide support and transfer the processing heat. Fig.3b shows the top-view of the equipment system. The dispenser duct transferred the powder, and the building chamber was used to print designed parts.

Fig. 4 shows SLM process strategy in this research. The rotation angle between two adjacent layers was 67° . The molten lines in one layer were parallel to each other and the length of one molten line was 5 mm. In order to keep the scanning speed of the laser constant during the whole printing process, the sky-writing mold was adopted. The red dotted

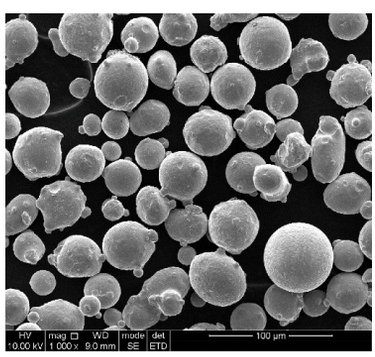

Fig.1 SEM morphology of gas-atomized 316L stainless steel powder

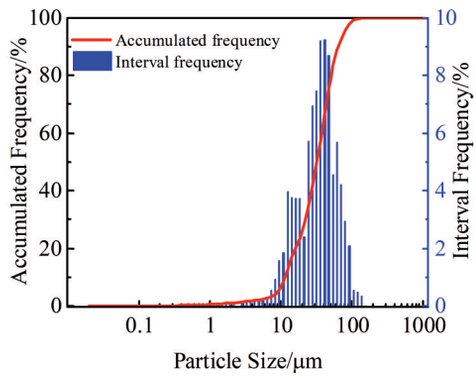

Fig.2 Particle size distribution of 316L stainless steel powder

Table 1 Chemical composition of 316L stainless steel powder (wt%)

C	Cr	Ni	Fe
0.01	16.94	10.22	Bal.

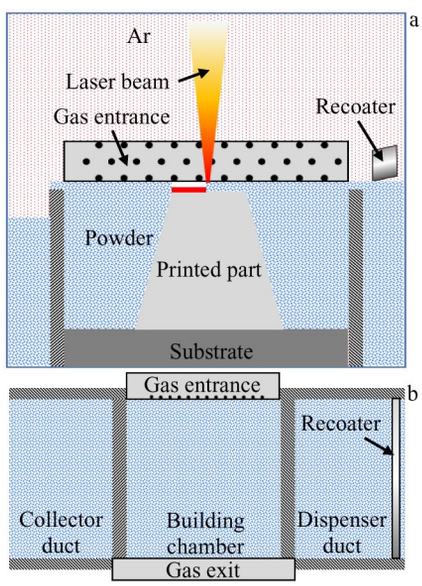

Fig.3 Schematic diagrams of profile (a) and top-view (b) of SLM preparation system

lines in Fig.4 present the zigzag moving route of laser beam in this mode, indicating that the laser beam is turned off and the scanning speed decreases after the laser beam leaves the melted area. When the scanning speed decelerated to 0 mm/s, the laser beam moved to an adjacent line immediately and the scanning speed was accelerated along the reverse direction in a row.

The volume energy density (E), namely the energy input per unit volume, can be calculated by Eq.(1)[12], as follows:

$$E = \frac{P}{SHL} \quad (1)$$

where E is energy density, P is the laser power, S is the laser scanning speed, H is hatch distance between two scanning lines, and L is the layer thickness.

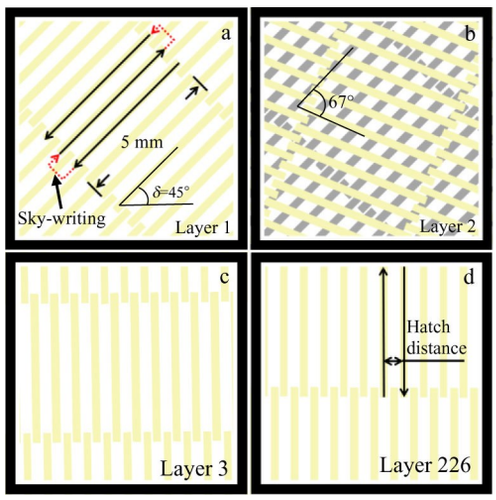

Fig.4 Schematic diagrams of SLM strategy

The main process parameters used in this study are summarized in Table 2. The laser power, hatch distance, and layer thickness were set as 275 W, 0.11 mm, and 50 μm, respectively, while the scanning speed varied from 800 mm/s to 1200 mm/s. The substrate temperature was heated to 353 K before SLM process. To prevent oxidation during the printing process, the process chamber was protected by argon atmosphere. In addition, a gas flow was adopted to prevent the laser beam from metal vapor[16]. The pressure difference between the gas entrance and gas exit was controlled at 0.56 MPa.

The model size was 8 mm×8 mm×11.23 mm. The schematic diagram of model and building directions is shown in Fig.5. The angle δ (Fig.4) between the molten lines and the front side of the model constantly changes at different layers. At Layer 1, δ=45°. At Layer 226 (the end of printing process), the molten lines are perpendicular to one side of the printed

Table 2 SLM process parameters

No.	Layer thickness, L/μm	Laser power, P/W	Hatch distance, H/mm	Scanning speed, S/mm·s^{-1}	Energy density, E/J·mm^{-3}
S1				800	62.5
S2				900	55.6
S3	50	275	0.11	1000	50.0
S4				1100	45.5
S5				1200	41.7

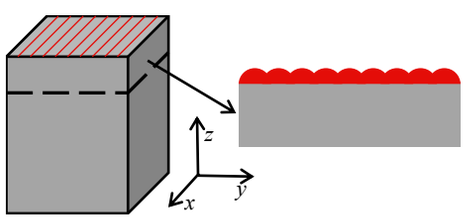

Fig.5 Schematic diagram of printed model

part. The top layer of model is presented in red (Fig.5), and its structure of molten pool without remelting could be observed.

Phase analysis was performed by X-ray diffractometer (XRD, DX-2000) with a graphite monochromator using Cu Kα radiation. The scanning rate was 0.06°/s at 2θ=20°–100° . The electron back-scattered diffractometer (EBSD) coupled with JEOL JMS-7900F SEM (SYNNETRY EBSD system) was used for microstructure observation and analysis. The microstructure was also characterized by optical microscope (OM). Before the metallographic analysis, the specimens were mechanically polished, chemically etched, and ultrasonic cleaned.

The density ρ can be evaluated by the Archimedes method. The relative density ρ_r can be calculated by Eq.(2), as follows:

$$\rho_r = \frac{\rho}{\rho_t} \quad (2)$$

where ρ_t is theoretical density. ρ_t can be calculated by the element composition.

Tensile strength test was performed by a material test machine (Shimadzu AG-10TA) at room temperature with crosshead speed of 2 mm/min. The hardness was tested via Vickers hardness tester (452SVA Wolpert Wilson) with load of 29.4 N and dwelling time of 15 s. The hardness tests were repeated at least five times.

Surface roughness was evaluated by an optical profiler (ContourGT-K) with the scanning area of 0.8 mm×0.6 mm.

2 Results and Discussion

2.1 Phase constitution and texture

XRD patterns of initial powder and SLMed specimens are shown in Fig.6. It can be seen that only face-centered cubic γ austenite is formed in the SLMed specimens under different scanning speeds. The diffraction peaks of SLMed specimens at 1200 and 1100 mm/s are similar to those of the raw 316L powder. In contrast, the diffraction peaks of specimens SLMed at 900 and 800 mm/s are obvious at (220) plane. This result suggests that the SLMed specimens under different scanning speeds have different crystallographic textures.

Fig. 7 shows inverse pole figures (IPFs) obtained from EBSD maps of SLMed specimens at scanning speed of 1200 and 800 mm/s and their corresponding pole figures. TD and RD represent the transverse direction and rolling direction, respectively. In Fig. 7a, the specimen SLMed at 1200 mm/s shows a relatively low texture degree. The relatively even distribution of red, green, and blue areas in IPFs indicates the relatively weak alignment of <001> , <101> , and <111> directions. This result is also supported by the {100}, {110},

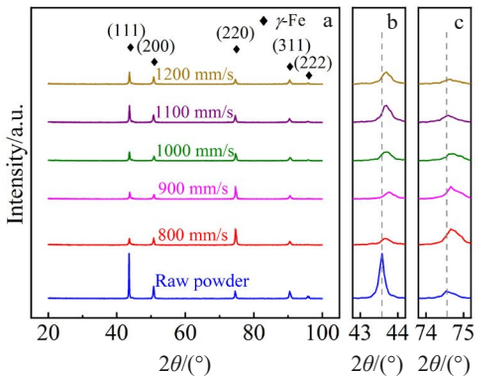

Fig.6 XRD patterns of raw 316L powder and SLMed specimens at different scanning speeds: (a) 2θ=20°–100°; (b) 2θ=43°–44°; (c) 2θ=74°–75°

and {111} pole figures. According to Fig. 7c, the specimen SLMed at 800 mm/s exhibits an obvious texture along <110> direction. This is supported by the {110} pole figure.

Different scanning speeds result in different laser energy densities, which leads to the evolution of microstructures[17]. It is reported that the low laser power of 100 W leads to the low texture degree, whereas the high laser power of 200 W leads to strong <001> texture for the 316L stainless steel[18].

2.2 Microstructure

Fig.8 shows the surface appearances and microstructures of specimens SLMed at different scanning speeds. At scanning speed of 800 mm/s, the surface morphology of the molten lines is regular, but the transverse cracks can be noticed on the surface of the molten lines (Fig. 8a). With increasing the scanning speed, the surface of molten lines is still regular

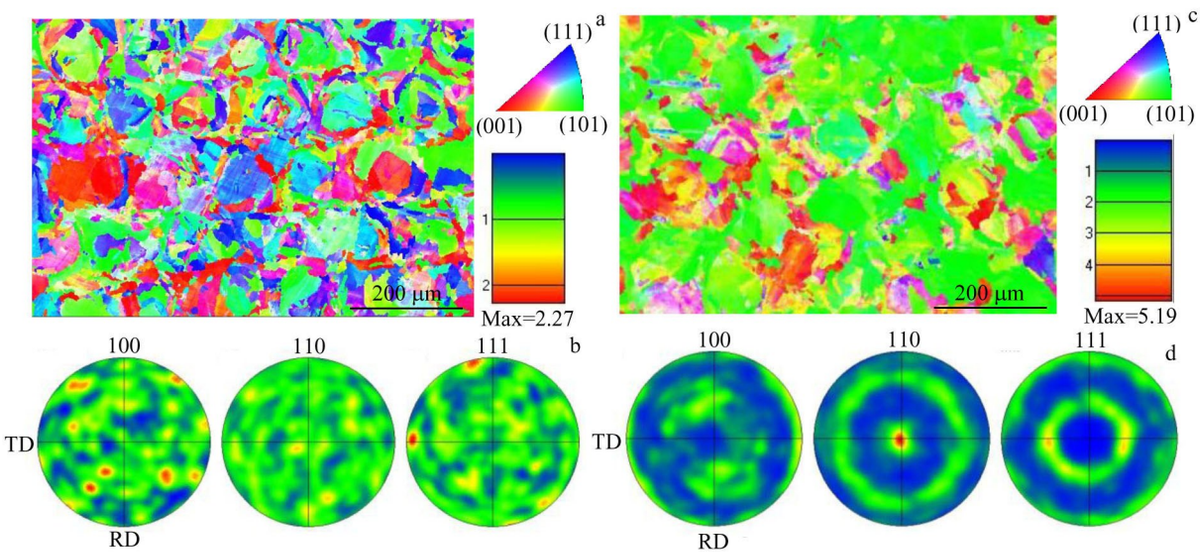

Fig.7 IPFs (a, c) and corresponding pole figures (b, d) of SLMed specimens at scanning speed of 1200 mm/s (a, b) and 800 mm/s (c, d)

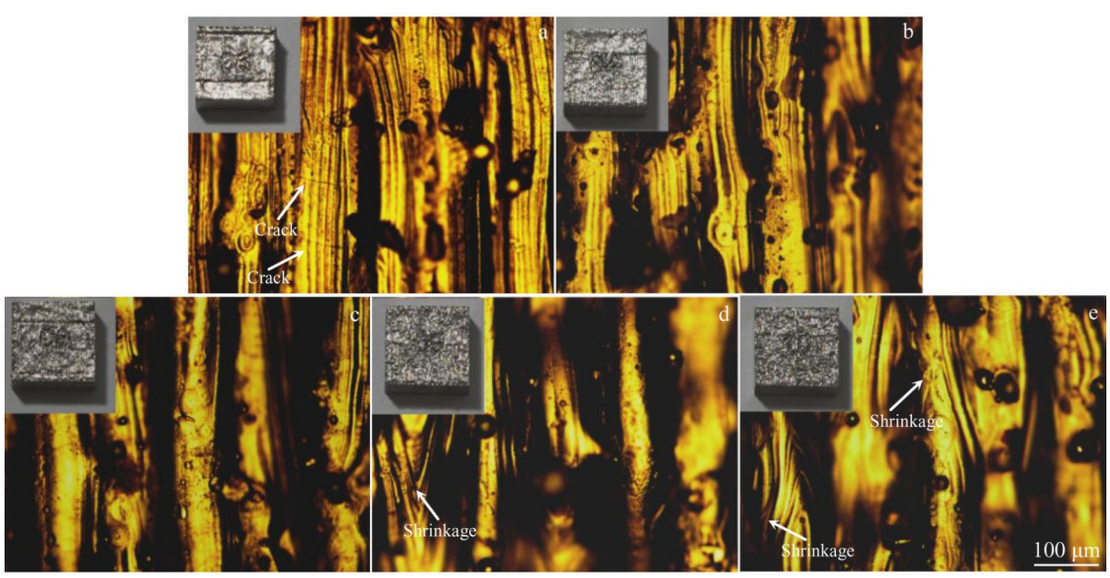

Fig.8 Surface appearances and microstructures of SLMed specimens at scanning speeds of 800 mm/s (a), 900 mm/s (b), 1000 mm/s (c), 1100 mm/s (d), and 1200 mm/s (e)

without cracks (Fig. 8b and 8c). As shown in Fig. 8d and 8e, the shrinkage appears in molten lines and it becomes more obvious with increasing the scanning speed.

Due to the influence of scanning speed, the molten lines have various surface morphologies. According to Eq. (1), the energy density E is decreased with increasing the scanning speed. Excessive energy input leads to the larger temperature gradients and higher cooling rates, resulting in the formation of transverse cracks[10], which agrees well with the observation in Fig. 8a. However, decreasing the energy input causes lower working temperature and consequently higher melt viscosity and surface tension of the molten liquid[19–20]. Therefore, with increasing the scanning speed, the liquid flow in the molten pool becomes more difficult, which causes more irregular molten lines[9] and even shrinkage (Fig.8d and 8e).

Fig. 9 shows the cross section microstructures of the molten pools without remelting. Typical fish scale-like structures can be observed in all specimens. As shown in Fig. 10, with increasing the scanning speed, the depth-to-width ratio of the molten pool is decreased from 1.07 to 0.64, indicating that the scanning speed alters the molten pool shape significantly. In addition, according to the cross section microstructures of the molten pools, when the scanning speed is low, the top surface of the molten pool is relatively flat. In contrast, with increasing the scanning speed, the top surface of the molten pool gradually becomes rough. This may be caused by the poor wettability of the molten pool[8].

2.3 Surface roughness

The surface roughness results are shown in Fig. 11. At scanning speed (S) of 800 mm/s, the average surface roughness R_a of specimen is 5.78 μm, which is the lowest among the surface roughness of these specimens. As the scanning speed rises to 900 mm/s, the average surface roughness rises slightly to 6.98 μm. With further increasing the scanning speed to 1000 mm/s, the average surface roughness is increased rapidly to 11.61 μm. The highest roughness of 22.79 μm is achieved at scanning speed of 1200 mm/s. Due to the insufficient energy input under high scanning speed, poor wettability and high viscosity occur during SLM process[21], leading to the unstable and wrinkled surface of the molten lines and resulting in the increase in surface roughness[10,14].

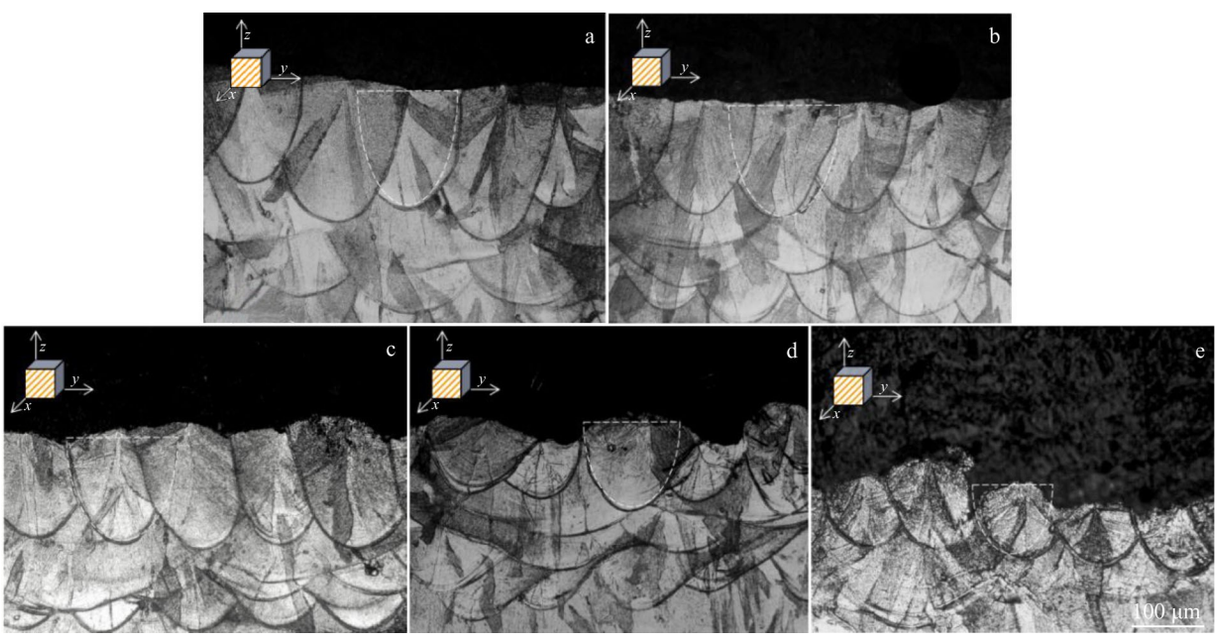

Fig.9 Cross section microstructures of molten pool in SLMed specimens at different scanning speeds without remelting: (a) 800 mm/s, (b) 900 mm/s, (c) 1000 mm/s, (d) 1100 mm/s, and (e) 1200 mm/s

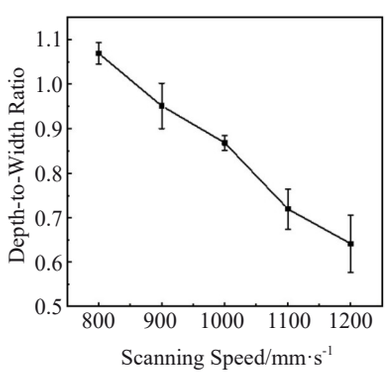

Fig. 10 Depth-to-width ratios of molten pools in SLMed specimens at different scanning speeds

2.4 Relative density and Vickers hardness

The relative density and Vickers hardness of specimens SLMed at different scanning speeds are shown in Fig.12.

The surface of printed parts for Vickers hardness test was perpendicular to the building direction. Obviously, with increasing the scanning speed, the Vickers hardness is firstly increased and then decreased, which is consistent with the

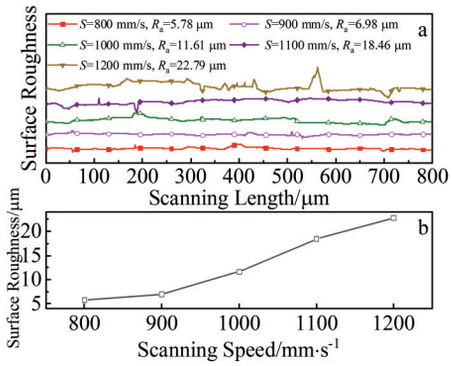

Fig.11 Distributions (a) and average value (b) of surface roughness of specimens SLMed at different scanning speeds

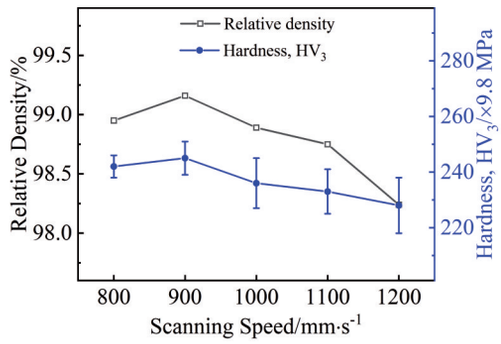

Fig.12 Relative density and Vickers hardness of specimens SLMed at different scanning speeds

trend of relative density. The peak hardness occurs at scanning speed of 900 mm/s. At scanning speed of 800 mm/s, the energy density is too high, so the pores form, as shown in Fig. 13a. Due to the increased porosity, the hardness is decreased. This is primarily due to the pore collapsing under load in the material[14,17]. With increasing the scanning speed to 900 mm/s, the relative density and hardness reaches the maximum value of 99.2% and 2401 MPa, respectively. With further increasing the scanning speed, the low input energy

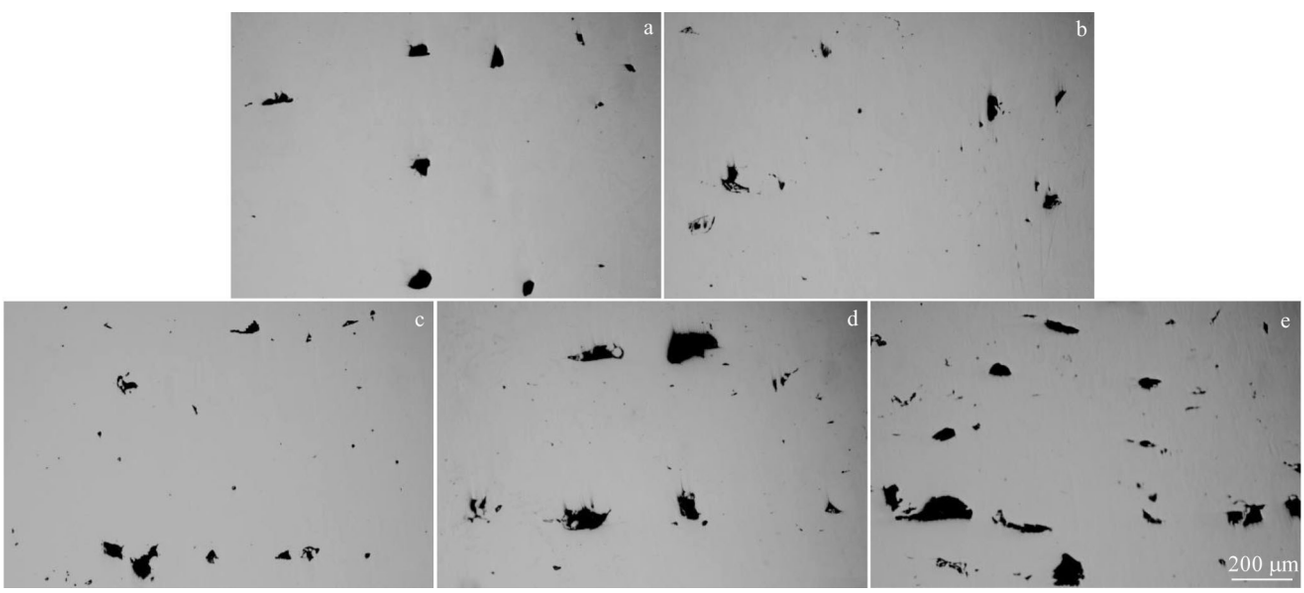

Fig.13 OM morphologies of SLMed specimens at scanning speeds of 800 mm/s (a), 900 mm/s (b), 1000 mm/s (c), 1100 mm/s (d), and 1200 mm/s (e)

causes the high viscosity of the molten pool, which leads to the incomplete spread of the molten liquid before solidification and decreases the fusion porosity (Fig.13c–13e), thus reducing the relative density and hardness[14].

2.5 Tensile behavior

Fig. 14 exhibits the stress-strain curves of different SLMed specimens. The highest yield strength (543 MPa) is achieved at scanning speed of 900 mm/s, whereas the highest elongation (48%) is obtained at scanning speed of 1000 mm/s. The appearance of cracks and pores within the printed specimens is detrimental to the mechanical properties of SLMed specimens[22]. Briefly, the SLMed specimens show a good combination of strength and ductility.

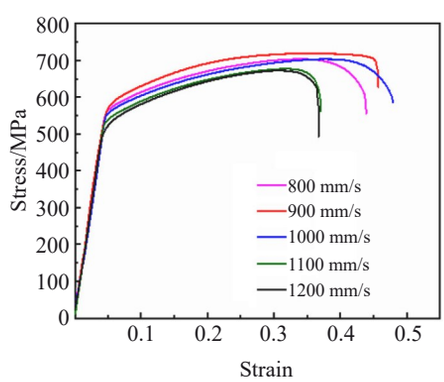

Fig.14 Stress-strain curves of SLMed specimens at different scanning speeds

3 Conclusions

1) The scanning speed significantly alters the molten pool shape of the 316L stainless steel part fabricated by selective laser melting. The depth-to-width ratio of molten pool is decreased from 1.07 to 0.64 with increasing the scanning speed.

2) The surface roughness is decreased with increasing the scanning speed. The lowest roughness of 5.78 μm is obtained at scanning speed of 800 mm/s, while the highest roughness of 22.79 μm is achieved at scanning speed of 1200 mm/s.

3) The optimal hardness (2401 MPa) and relative density (99.2%) are achieved at the scanning speed of 900 mm/s. The highest yield strength (543 MPa) is also obtained at scanning speed of 900 mm/s, whereas the highest elongation (48%) is obtained at scanning speed of 1000 mm/s.

References

1 Kong D C, Dong C F, Ni X Q *et al. Applied Surface Science*[J], 2020, 504: 144 495

2 Song B, Zhao X, Li S *et al. Frontiers of Mechanical Engineering*[J], 2015, 10(2): 111

3 Liu M, Li J, Zhang Y X *et al*. *Rare Metal Materials and Engineering*[J], 2021, 50(11): 4165

4 Lu Y J, Wu S Q, Gan Y L *et al. Optics & Laser Technology*[J], 2015, 75: 197

5 Liverani E, Fortunato A, Leardini A *et al. Materials & Design*[J], 2016, 106: 60

6 Lodhi M J K, Deen K M, Haider W. *Materialia*[J], 2018, 2: 111

7 Yadroitsev I, Bertrand P, Smurov I. *Applied Surface Science*[J], 2007, 253(19): 8064

8 Le K Q, Tang C, Wong C H. *International Journal of Thermal Sciences*[J], 2019, 145: 105 992

9 Bertoli U S, Wolfer A J, Matthews M J *et al. Materials & Design*[J], 2017, 113: 331

10 Guo M, Gu D D, Xi L X *et al. International Journal of Refractory Metals and Hard Materials*[J], 2019, 79: 37

11 Sun Z J, Tan X P, Tor S B *et al. NPG Asia Materials*[J], 2018, 10(4): 127

12 Song Y N, Sun Q D, Guo K *et al. Materials Science and Engineering A*[J], 2020, 793: 139 879

13 Tucho W M, Lysne V H, Austbø H *et al. Journal of Alloys and Compounds*[J], 2018, 740: 910

14 Cherry J A, Davies H M, Mehmood S *et al. The International Journal of Advanced Manufacturing Technology*[J], 2014, 76(5–8): 869

15 Nguyen Q B, Luu D N, Nai S M L *et al. Archives of Civil and Mechanical Engineering*[J], 2018, 18(3): 948

16 Bidare P, Bitharas I, Ward R M *et al. Acta Materialia*[J], 2018, 142: 107

17 Thomas N, Stefan L, Andre R. *Metallurgical and Materials Transactions B*[J], 2013, 44(4): 794

18 Kurzynowski T, Gruber K, Stopyra W *et al. Materials Science and Engineering A*[J], 2018, 718: 64

19 Li R D, Shi Y S, Liu J H *et al. Powder Metallurgy and Metal Ceramics*[J], 2009, 48: 186

20 Zhao C, Parab N D, Li X X *et al. Science*[J], 2020, 370(6520): 1080

21 Gu D D, Shen Y F. *Materials & Design*[J], 2009, 30(8): 2903

22 Gong H J, Rafi K, Gu H F *et al. Materials & Design*[J], 2015, 86: 545

扫描速度对激光选区熔融316L不锈钢表面粗糙度和力学性能的影响

毛彬洋，刘　颖，叶金文，陈正杰

(四川大学 材料科学与工程学院，四川 成都 610065)

摘　要：采用选区激光熔融法在不同扫描速度下制备了316L不锈钢成型件，通过物相分析、金相观察、拉伸试验、维氏硬度试验和表面粗糙度试验，研究了扫描速度对成型件相组成、熔池形态、表面粗糙度、密度和力学性能的影响。结果表明，在不同的扫描速度下（800~1200 mm/s）样品均能成功打印。此外，随着扫描速度的增加，未重熔的熔池深宽比降低，表面粗糙度从5.78 μm增加到22.79 μm。当扫描速度为800 mm/s时，裂痕出现；当扫描速度超过1100 mm/s时，出现收缩纹路。当扫描速度为800 mm/s时，由于激光输入能量过高，样品具有较高的孔隙率。当扫描速度为900 mm/s时，样品具有最佳的维氏硬度（2401 MPa）和最高的相对密度（99.2%）。

关键词：选区激光熔融；316L；表面粗糙度；扫描速度

作者简介：毛彬洋，男，1994年生，硕士，四川大学材料科学与工程学院，四川 成都 610065，电话：028-85405332，E-mail：zhonghmao@163.com